Earthq Eng & Eng Vib (2019) 18: 703-717 **DOI**: https://doi.org/10.1007/s11803-019-0531-8

Mapping of ground motion amplifications for the Fraser River delta in Greater Vancouver, Canada

Byungmin Kim†

Ulsan National Institute of Science and Technology, 50 UNIST-gil, Ulju-gun, Ulsan 44919, Republic of Korea

Abstract: The Fraser River delta in Greater Vancouver, Canada consists of deep soft deposits of silts and clays, and it is well known that the deep soil deposits can amplify the low frequency contents of ground motions. This study aims to investigate the effects of deep soil deposits in the delta on ground motion amplifications by using thorough site response simulations that account for the full soil profiles and a suite of recorded ground motions that covers a wide range of intensity levels. Based on both equivalent-linear and nonlinear site response simulations, the effects of soil depth (represented by natural period of the soil, T_S) on ground motion amplifications for various spectral periods are clearly demonstrated. The ground motion amplification maps for various spectral periods and rock ground motion intensity levels are also generated to be used in the regional seismic hazard assessment for infrastructure. It is found that ground motions for long periods are substantially amplified in the center of the delta, while those for short periods are de-amplified when input rock motions are large.

Keywords: Fraser River delta; ground motion amplification; deep soil deposits; site response analysis; basin depth

1 Introduction

The Fraser River delta is located in southwestern British Columbia which is one of the most earthquake-prone regions in Canada, and underlain by Tertiary volcanic and sedimentary rocks. This bedrock surface is overlain by Pleistocene glacial deposits (Cassidy and Rogers, 1999). The Holocene sediments including sand, silt, clay, and peat were deposited over a Pleistocene surface during the past 10,000 years after the last glaciation (Clague *et al*., 1998), and the depth extends down to 300 m (Hunter and Christian, 2001). Thicknesses of the Holocene sediments are shown in Fig. 1. Depth to Tertiary bedrock is as deep as 800 m (Britton *et al*., 1995). Figure 1 shows surficial geology within the vicinity of the delta. There is sharp contrast between soft sediments within the delta and tills (known as firm ground) in the vicinity. It is widely recognized that site responses and ground motion amplifications are dependent on the subsurface shear-wave velocity (V_S) profile, and long period motions are expected to be significantly amplified due to the deep sediments (e.g., Ewald *et al*., 2006; Frankel *et al*., 2009; Wang *et al*., 2013; Chenari and Bostani Taleshani, 2016; Liu *et al*., 2016; Liang *et al*., 2017; Li *et al*., 2018)

The Fraser River delta has many important infrastructure including the Vancouver International Airport (which include a control tower, monorails, and runways), Boundary Bay Airport, port facilities

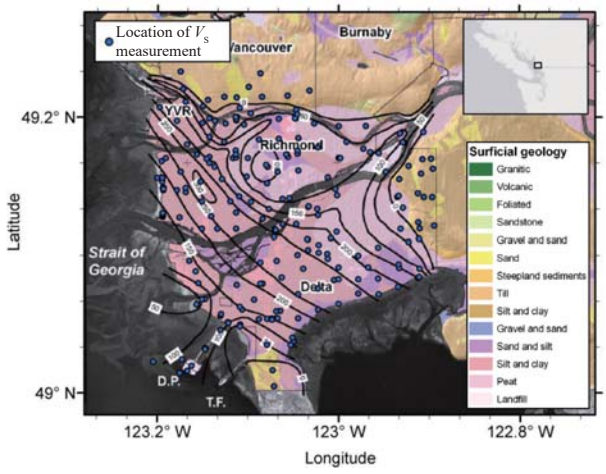

Fig. 1 Surficial geology of Fraser River delta (after Mazzotti *et al*., 2009) and locations of V_S profile measurements. The contour lines represent thicknesses of Holocene sediments in meters

Correspondence to: Byungmin Kim, Ulsan National Institute of Science and Technology, 50 UNIST-gil, Ulju-gun, Ulsan 44919, Republic of Korea
Tel: +82 52 2172823; Fax: +82 52 2172809
E-mail: byungmin.kim@unist.ac.kr
†Assistant Professor

Supported by: 2018 Research Fund (1.170059.01) of UNIST (Ulsan National Institute of Science and Technology) and the National Research Foundation of Korea (NRF) with a grant from the Korean government (MSIT) (NRF-2017R1C1B5074430)
Received March 13, 2018; **Accepted** January 25, 2019

(including Deltaport), transportation networks (railways and highways), high-rise buildings, bridges, and the immersed tube George Massey Tunnel, which are usually considered to have long natural periods. In addition, the City of Richmond has a large population (207,500 as of 2014, http://www.richmond.ca/discover/about/demographics.htm). Therefore, ground motion amplifications at long periods are especially of concern for the Fraser River delta.

There have been several studies on ground motion amplifications for the Fraser River delta. Cassidy and Rogers (1999) investigated ground motion amplifications in the Fraser River delta using the ground motions recorded at soft soil sites and nearby rock sites during the 1996 *M*5.1 Duvall, Washington and 1997 *M*4.3 Georgia Strait earthquakes. Using these two events, Atkinson and Cassidy (2000) estimated ground motion amplifications as ratios of the Fourier spectra measured on the ground surface to the spectra of the inferred rock motions. However, the rock ground motions used by these two studies were weak with peak ground accelerations (PGAs) ranging from 0.0014 g to 0.0061 g. Finn *et al*. (2003) evaluated one-dimensional (1D) and 2D site response analyses using the ground motions recorded at strong motion stations in the Fraser River delta during the 1996 *M*5.1 Duvall, Washington earthquake. However, the rock ground motions used in their study were weak with PGA values of approximately 0.0047 g. Uthayakumar and Naesgaard (2004) used 1D equivalent-linear site response analyses to estimate the ground motion amplifications at four specific sites within the Fraser River delta. They scaled the ground motions recorded in California, United States, to match the design spectrum, and considered the PGA values of input motions of 0.5 g and 0.23 g. However, they considered that the top of the Pleistocene sediments as an elastic half space, and did not account for the effect of Pleistocene sediments in the site response analyses. Recently, Molnar *et al*. (Molnar *et al*., 2014a, b) investigated the effect of a 3D velocity structure in Georgia Basin, Greater Vancouver, Canada on site amplifications for long-period ground motion velocities using finite-difference modeling of wave propagation for both subduction zone and shallow blind-thrust scenario earthquakes. However, the velocity structure used in their study considered the V_S of Holocene deltaic sediments of the Fraser River delta to be 625 m/s.

This study is intended to overcome the limitations of the previous studies by accounting for full soil profiles (including both Holocene and Pleistocene deposits), and by developing ground motion amplifications at various spectral periods for a wide range of input PGA values using both 1D equivalent-linear (EL) and nonlinear (NL) site response simulations. Ground motion amplifications are computed from six generic Vs profiles, and validated with the NGA-West2 amplification models. Finally, the computed to amplifications are applied to the Fraser River delta to create amplification maps. While 3D effects need to be considered, the 3D simulation tools are not well validated yet due to a lack of data within the basin (especially near the basin edges). Therefore, the results of this study will provide important information until a reliable 3D simulation is conducted in the future. This study only considers ground motions generated by shallow crustal earthquakes because the site response analysis is not validated for the long-duration ground motions generated by subduction zone earthquakes (e.g., Kim and Hashash, 2013).

2 1D site response analysis

2.1 Shear-wave velocity profiles

Shear-wave velocity (V_S) profile data were collected from Hunter *et al*. (1998). Locations of the data are shown in Figure 1. Hunter *et al*. (1998) used refraction test, borehole logging, and standard penetration test (SPT) to measure V_S for relatively shallow depths (up to 300 m), and a velocity analysis to estimate V_S for greater depths. Log mean ($\mu_{\ln}$) and log mean ± one log standard deviation ($\sigma_{\ln}$) of the measured V_S profiles are also shown in Fig. 2. For shallow profiles (Figure 2a), soft soils and stiff soils are separated.

Figure 3 combines both shallow and deep V_S profiles. Six generic V_S profiles were proposed based on the log mean ($\mu_{\ln}$) and log mean ± one log standard deviation ($\sigma_{\ln}$) of the measured data. Generic profiles #1, #2, and #3 follow $\mu_{\ln} - \sigma_{\ln}$, $\mu_{\ln}$, and, $\mu_{\ln} + \sigma_{\ln}$, respectively, of both shallow and deep profiles. The shallow parts of the profiles (up to 100 m) were vertically connected to the deeper profiles, resulting in steady V_S values over certain depths. This is also observed in one of the two generic V_S profiles used by Atkinson and Cassidy (2000). Generic profile #4 is adopted from Atkinson and Cassidy (2000). The V_S of this profile follows $\mu_{\ln} - \sigma_{\ln}$ of shallow stiff profiles at depth < 10 m and increase with a constant gradient up to a depth of 600 m. Generic profile #5 follows $\mu_{\ln}$ of shallow stiff profiles at depth < 10 m and $\mu_{\ln} + 2\sigma_{\ln}$ of deep profiles. Generic profile #6 follows $\mu_{\ln}$ of shallow stiff profiles up to the depth of 50 m. The values of time-averaged V_S in the upper 30 meters (V_{S30}) for six generic profiles vary from 138.3 m/s to 505.4 m/s as listed in Table 1.

Britton *et al*. (1995) reported that the Tertiary bedrock is as deep as 800 m. Hunter *et al*. (1997) reported that the V_S near the surface of the Tertiary bedrock is approximately 1.5 km/s or greater. The data in Fig. 3 show a gradient change in V_S at about a depth of 800 m, and the V_S at this depth is approximately 1.7 km/s. Therefore, 1.7 km/s was considered as a bedrock V_S. In the simulation, the bedrock is modeled with the elastic half-space because rock outcrop motions are used as

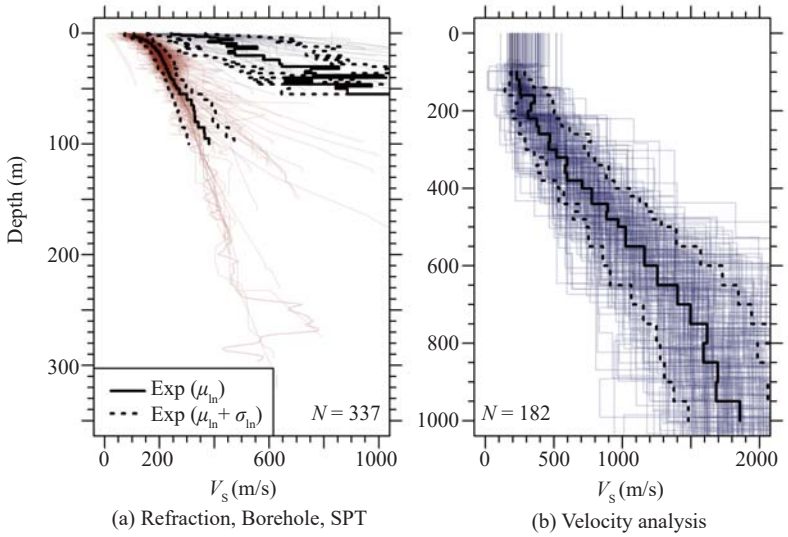

Fig. 2 Shear-wave velocity profile data within the Fraser River Delta from (a) refraction, borehole, and SPT techniques, and (b) velocity analysis technique (Hunter *et al*., 1998). Log mean (μ_{ln}) and log mean ± one log standard deviation (σ_{ln}) are also shown

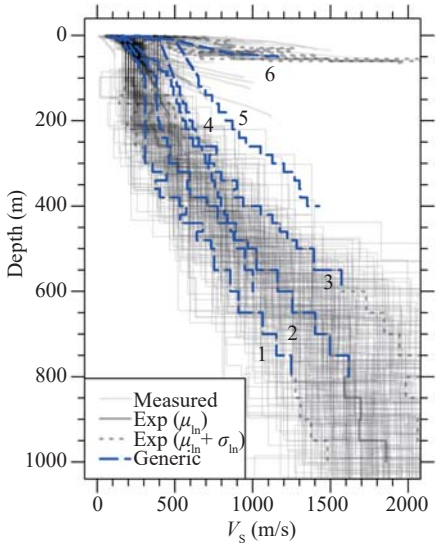

Fig. 3 Six generic V_S profiles based on the measured data

input ground motions in this study.

Various combinations of sediment thicknesses were considered. The thicknesses of Holocene sediments and depths to Tertiary bedrock considered in this study are shown in Table 1. The softer profiles have deeper profiles and vice versa. Therefore, a total of 21 V_S profiles were used in site response simulations.

2.2 Soil types and Nonlinear soil properties

Holocene sediments in the Fraser River Delta consist of unconsolidated silts, sands, and clayey silts. The depth of the Holocene sediments varies from a few meters to 300 m (Hunter *et al*., 1997). The Holocene sediments are overlying the Pleistocene deposits, which mainly consist of glacial tills. The Tertiary bedrock is overlain by the Pleistocene deposits.

The 32 geology logs from Hunter *et al*. (1998) were analyzed to estimate the proportions of sands and silts within the Holocene sediments as shown in Fig. 4. The depths with more than 30% sand layers were considered to be sand layers in the generic profiles. Compositions of soil layers for the six generic profiles are shown in Fig. 5.

The generic modulus reduction and damping curves of Darendeli (2001), which are considered to

Table 1 V_{S30}, Holocene sediment thickness, depth to Tertiary bedrock, and natural period for generic profiles

Generic profile no.	V_{S30} (m/s)	Holocene sediment thickness (m)	Depth to Tertiary bedrock (m)
1	138.3	300	400 (5.5)*, 600 (6.7), 800 (7.6)
2	170.0	150	200 (2.7), 400 (4.3), 600 (5.1), 800 (5.8)
3	207.5	50	100 (1.4), 200 (2.1), 400 (3.2), 600 (3.8)
4	330.0	10	50 (0.6), 100 (1.0), 200 (1.7), 400 (2.8), 600 (3.7)
5	454.8	10	50 (0.4), 100 (0.7), 200 (1.3), 400 (2.0)
6	505.4	10	50 (0.3)

*Natural period (in s) are shown in the parentheses

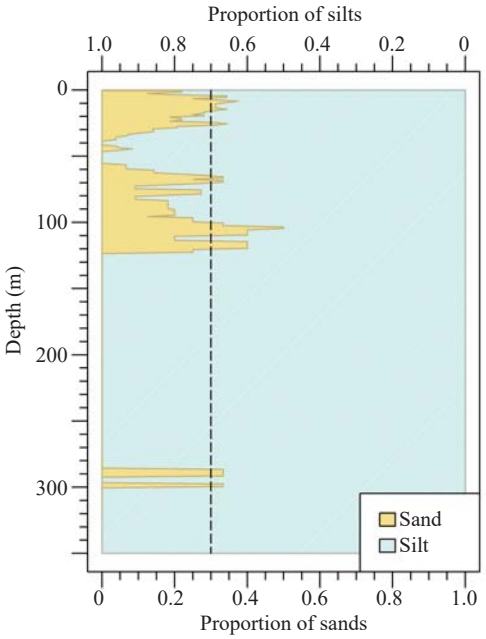

Fig. 4 Proportions of silts and sands within Holocene deposits based on geology logs from Hunter *et al*. (1998)

be an improvement over earlier curves, were used with the following material properties. The unit weights for sands, silts/clays, and Pleistocene sediments are considered to be 18.6, 17.2, and 21.6 kN/m^3 according to Uthayakumar and Naesgaard (2004). The over-consolidation ratio (OCR) of unity is assumed for all the layers. For silts/clays, the plasticity index (PI) of 5 is used for depths smaller than 25 m, 10 for depths between 25 m and 120 m, and 20 for depths between 120 m and 300 m, based on Dallimore *et al*. (1996), Anderson *et al*. (2007), and Wijewickereme (2010) . The shear strength of $0.22\sigma'_{v0}$ is used for Profiles 1 through 4 assuming soft silts (Ladd 1991), and $1\sigma'_{v0}$ for Profiles 5 and 6 assuming stiff silts. For sands, the shear strength is estimated using $\sigma'_{v0}\cdot\tan(\phi)$ where the friction angle, ϕ, is assumed to be 20° for Profiles 1 through 5, and 45° for Profile 6. For the Pleistocene sediments, the PI is assumed to be 35 for depths smaller than 100 m and 50 for depths greater than 100 m (Dallimore *et al*., 1996; Anderson *et al*., 2007). Figure 6 shows examples of the modulus reduction and damping curves for selected soil layers.

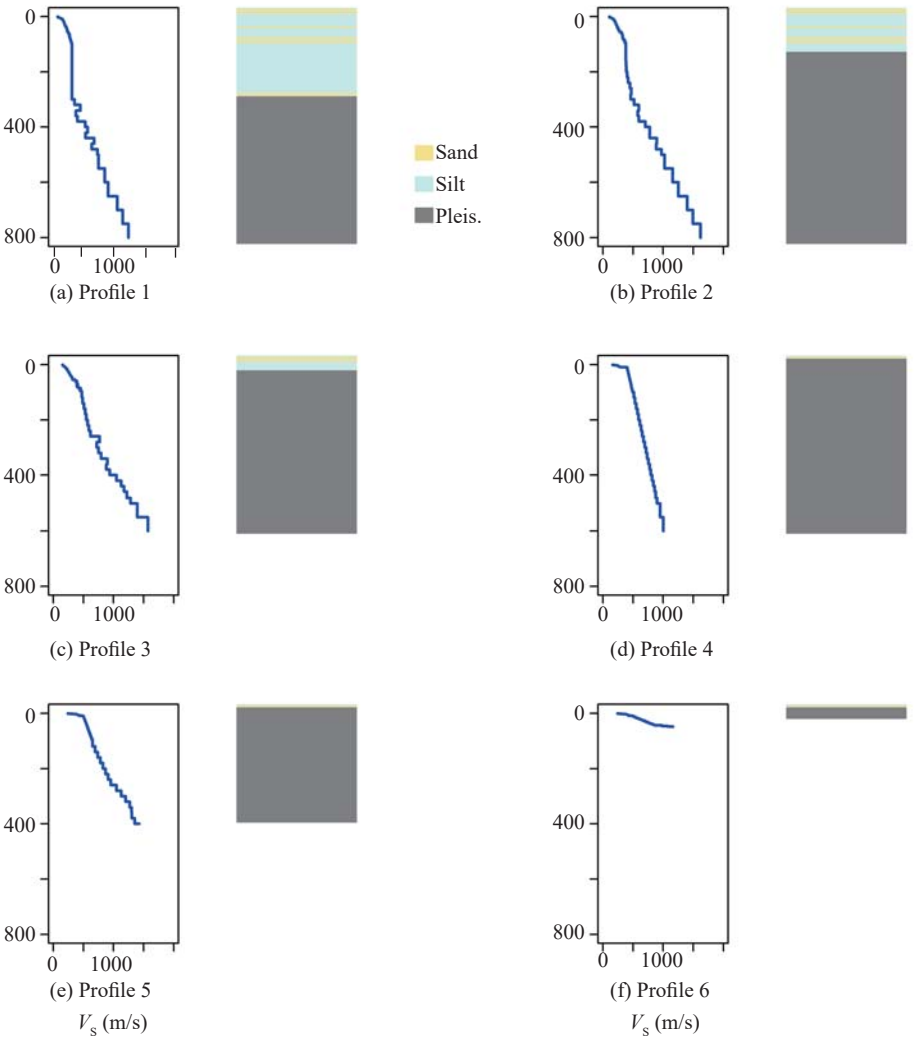

Fig. 5 Generic profiles and assigned soil types

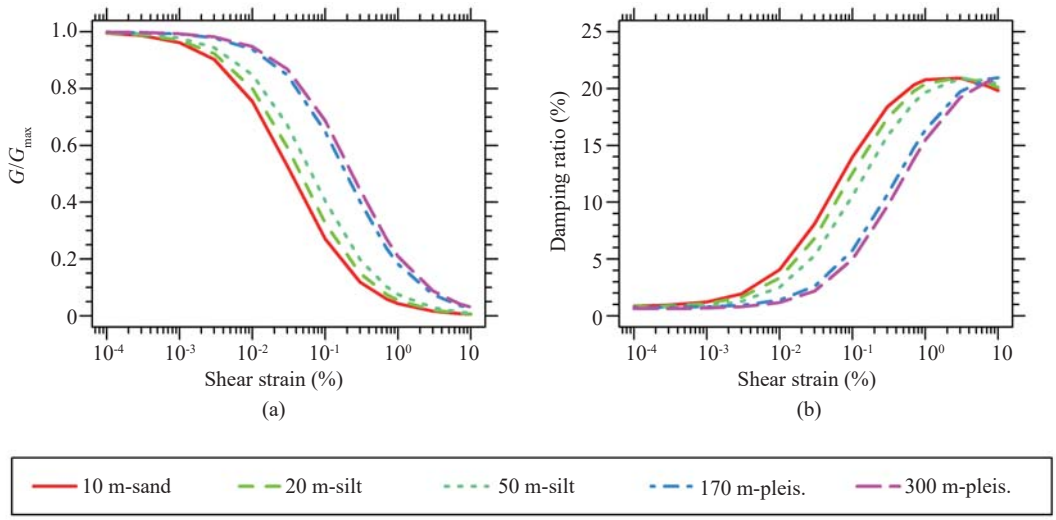

Fig. 6 Modulus reduction and damping curves by Darendeli (2001) for different depths and soil types

2.3 Input motions

Strong ground motions measured in California, United States, were collected from the NGA-West2 database (Ancheta *et al*., 2014) to be used as input ground motions in site response simulations. The motions measured at very stiff soil and rock conditions (with $V_S > 610$ m/s) and with PGA > 0.01 g were considered. Figure 7 shows 5 % damped spectral accelerations of the collected ground motions. The PGA ranges from 0.01 g to approximately 2 g. The log mean of PGA is about 0.1 g. It was checked that spectral shapes of the select input motions with $V_S < 1{,}000$ m/s and those with $V_S \geq 1{,}000$ m/s are similar. All the motions used in this study are for shallow crustal earthquakes, and deep crustal, inslab, and subduction zone earthquake motions are not considered for the reasons mentioned earlier.

2.4 Site response analysis methodology

Both EL and NL 1D site response simulations were performed with the program DEEPSOIL v6.1 (Hashash *et al*., 2015). A total of 10,332 analyses (246 motions × 21 V_S profiles × 2 analysis methods, EL and NL) were performed. The General Quadratic/Hyperbolic (GQ/H) model (Groholski *et al*., 2016) implemented in DEEPSOIL v6.1 (Hashash *et al*., 2015) was used as a nonlinear constitutive model. A frequency-independent damping model was used to account for viscous damping at very small strains as described in Phillips and Hashash (2009). The nonlinear constitutive soil model properties were selected to fit the Darendeli (2001) target curves using the reduction factor procedure proposed by Phillips and Hashash (2009). The fitted modulus reduction and damping curves used in NL analyses were used for EL analyses as well.

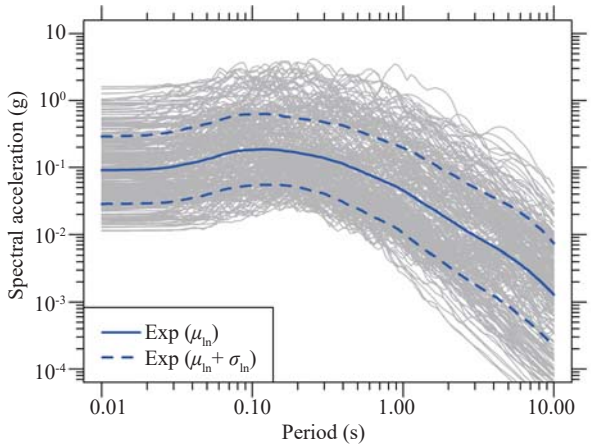

Fig. 7 5% damped response spectra of all selected input ground motions

The equivalent-linear and nonlinear analyses have their own advantages and disadvantages, resulting in different results depending on intensities of input motions and soil conditions (e.g., Kim *et al*., 2016). Although there is increasing consensus that nonlinear site response analyses better estimates surface ground motions (e.g., Kaklamanos *et al*., 2013), there is still controversy on how much weights should be given to these two analysis methods. In this study, equal weights are assigned to the results from equivalent-linear and nonlinear site response analyses. In order to evaluate the effects of analysis methods, mean values of ground motion amplifications, $\ln(Sa^{surface}/Sa^{rock})$ are presented separately for the equivalent-linear and nonlinear site response analyses in the Appendix.

3 Site response analysis results

Figure 8 shows natural logarithm of ground motion amplifications with respect to PGA of the rock motion (PGA^{rock}) for nine selected periods (T). The ground motion amplification is defined as the ratio of spectral

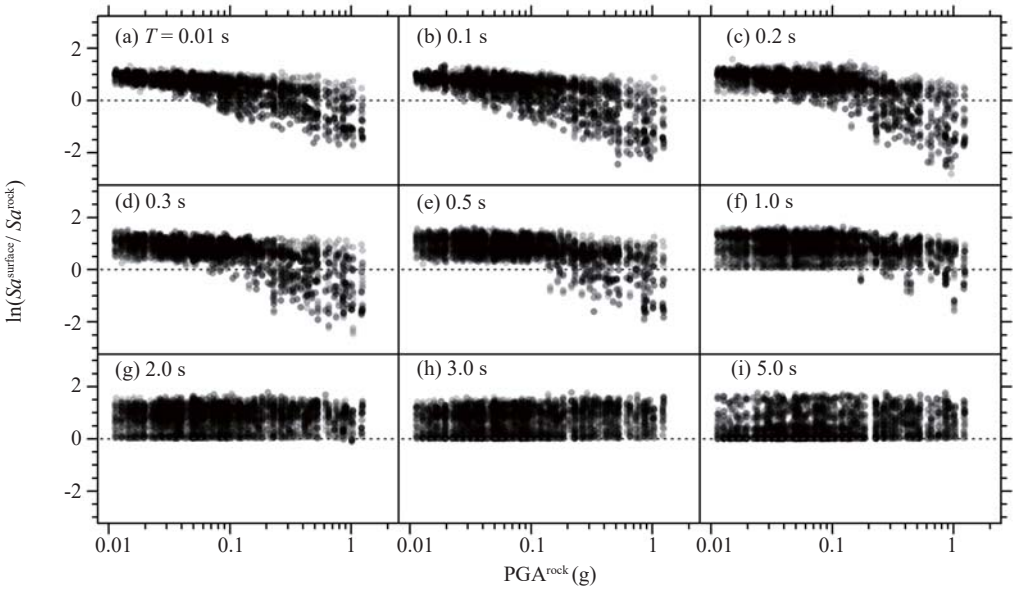

Fig. 8 Natural logarithm of ground motion amplification, ln($Sa^{surface}/Sa^{rock}$), versus PGA^{rock} for nine selected periods

acceleration on the ground surface computed by the 1D site response analysis ($Sa^{surface}$) to that within rock used as an input of the analysis (Sa^{rock}). The amplifications computed by both EL and NL analyses were equally weighted.

For short periods (T = 0.01 s – 0.5 s), the amplification ($Sa^{surface}/Sa^{rock}$) is as large as approximately 4.5 when PGA^{rock} is small, decreases with PGA^{rock}, and becomes less than unity at large PGA^{rock}, which indicates de-amplification. However, at long periods (T = 2.0 s – 5.0 s), the amplification varies from unity to approximately 7.3, but does not change with PGA^{rock}.

3.1 Comparison with the NGA-West 2 Models

In the study area, there are only a few measurements of earthquake ground motions with very low intensities (Cassidy *et al*., 1997; Finn *et al*., 2003; Cassidy and Rogers, 2004; Ancheta *et al*., 2014), which are not appropriate to use for validation of the site response simulations. Therefore, the results were compared with previous Ground Motion Prediction Equations (GMPEs) for validation purposes. Among the currently available GMPEs (e.g., Wong *et al*., 2002; Sihua and Lung, 2004; Graizer, 2016; Kim and Shin, 2017; Vaez Shoushtari *et al*., 2018), the amplifications computed by this study were compared to the site amplification models proposed by the Next Generation Attenuation relationships for Western North America 2 (NGA-West2) Ground Motion Prediction Equations (GMPEs), which are considered to be applicable to Western North America (i.e., Abrahamson *et al*., 2014; Boore *et al*., 2014; Campbell and Bozorgnia, 2014), Chiou and Youngs, 2014). These models are developed based on the ground motion data measured in active crustal regions including California, Japan and some European countries. In addition to empirical data, the ASK14, BSSA14, and CB14 GMPEs used the data from equivalent-linear site response simulations conducted by Walling *et al*. (2008) to constrain the amplification models. The CY14 GMPE only used empirical data. The depth terms for all of these models were developed using the depth data for California and Japan.

Figure 9 shows the mean and mean ± one standard deviation of ln($Sa^{surface}/Sa^{rock}$) for the subset of profiles with a depth to bedrock of 100 m and a V_{S30} of 455 m/s with respect to PGA^{rock} for nine selected periods, compared with the amplifications by the four NGA-West2 GMPEs. Note that the standard deviation values are small because the data shown here is a subset of the entire data. The ASK14, BSSA14, and CY14 models use the 1 km/s V_S horizon ($Z_{1.0}$), and CB14 $Z_{2.5}$ as input parameters. Therefore, assuming the amplification from $Z_{1.5}$ to $Z_{1.7}$ (bedrock V_S of this study is 1.7 km/s) is negligible, the $Z_{1.0}$ and $Z_{2.5}$ values that are equivalent to $Z_{1.5}$ of 100 m were estimated using the relationships proposed by Campbell and Bozorgnia (2013). Overall, the amplifications by this study are in good agreement with those by the NGA-West2 models. The amplifications at short periods ($T \leq$ 0.1 s) are slightly larger than those by the NGA-West2 amplifications, but at other periods they are in a range of the NGA-West amplifications.

When the soil profile becomes softer (V_{S30} = 208 m/s and depth to bedrock = 100 m), the nonlinearity in amplification vs. PGA^{rock} becomes more evident at short periods ($T \leq$ 1.0 s) and amplifications become larger at long periods (T > 1.0 s) as shown in Fig. 10. The amplification nonlinearity at short periods by this study is slightly stronger than that by the NGA-West models. At long periods, the differences among the NGA-West2

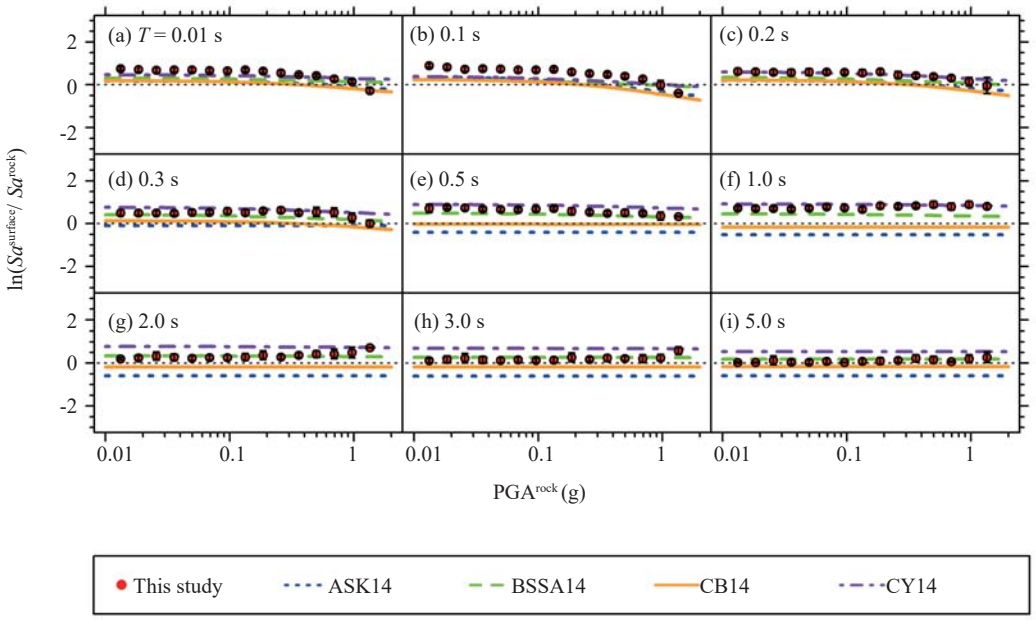

Fig. 9 Amplifications for profiles with a depth of 100 m and a V_{S30} of 455 m/s compared with the amplifications by NGA-West2 GMPEs

amplifications become larger compared to the stiffer site (with a V_{S30} of 455 m/s), and the amplifications by this study remains within the range of the NGA-West2 amplifications.

Figures 11 and 12 show the mean and mean ± one standard deviation of $\ln(Sa^{surface}/Sa^{rock})$ for the subset of profiles with a depth to bedrock of 500 m and a V_{S30} of 455 m/s and 208 m/s, respectively. Similarly with the cases for a depth to bedrock of 100 m, the amplifications estimated by this study are in good agreement with those by the NGA-West2 GMPEs. It is also notable that the amplifications at long periods have increased due to the deep soil deposits.

3.2 Effects of site period

In order to account for both soil conditions and thickness for the characterization of ground motion amplifications, this study used the natural period of soil deposits (T_S, also known as the site period), which is defined as:

$$T_S = \sum \frac{4H_i}{V_{S,i}} \quad (1)$$

where H_i is a soil thickness at ith layer, and $V_{S,i}$ is a V_S at ith layer. The estimated site periods for all 21 soil profiles vary from 0.3 s to 7.6 s.

Figure 13 shows the mean values of $\ln(Sa^{surface}/Sa^{rock})$ grouped by the site period, which clearly demonstrates the effects of site period in ground motion amplifications. At short periods ($T \leq 0.2$ s), amplifications decrease with PGA^{rock}, and also decrease with T_S, particularly when the PGA^{rock} is large. For example, the amplification is unity when PGA^{rock} is approximately 1 g and T_S is between 0.3 s and 1.5 s, but decreases to approximately 0.14 when T_S is between 4 s and 8 s. This ground motion de-amplification phenomenon is also presented in the ground motion amplification maps in the later section. At long periods ($T \geq 2$ s), amplifications barely change with PGA^{rock}, and increase with T_S. At $T = 5$ s, the amplification is about unity when T_S is between 0.3 s and 1.5 s over a range of PGA^{rock}, and increase to approximately 4.5 when T_S is between 4 s and 8 s. For intermediate periods ($T = 0.3$ s – 1 s), it is observed that these two amplification features are mixed. The amplifications increase with T_S for the small PGA^{rock} range, and decrease with T_S for the large PGA^{rock} range. The smoothed amplifications are shown by dashed lines. The simulation data for each T_S range are shown in the Appendix.

4 Ground motion amplification map

In order to generate the ground motion amplification map for the Fraser River delta in Greater Vancouver, Canada using the ground motion amplifications estimated by this study, it is necessary to develop a site period (T_S) map for this area. For each of the V_S profiles (as shown in Fig. 2), T_S was calculated using Eq. (1), and T_S values at all locations were spatially smoothed using the ordinary kriging method. The final T_S map is shown in Fig. 14. Outside of the delta basin where the firm grounds (Pleistocene deposits) are exposed on the

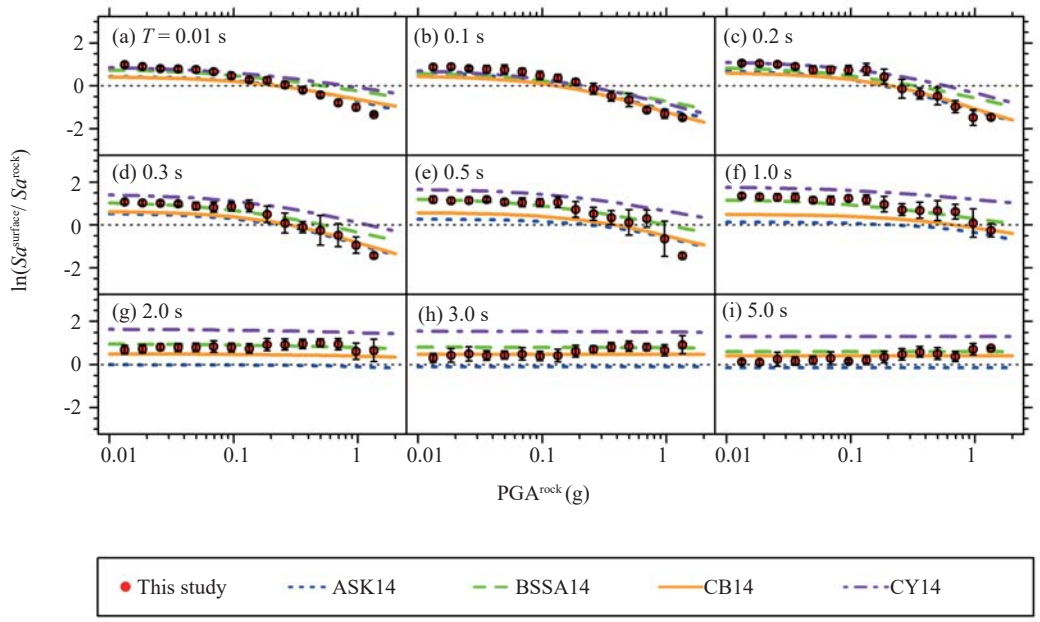

Fig. 10 Amplifications for profiles with a depth of 100 m and a V_{S30} of 208 m/s compared with the amplifications by NGA-West2 GMPEs

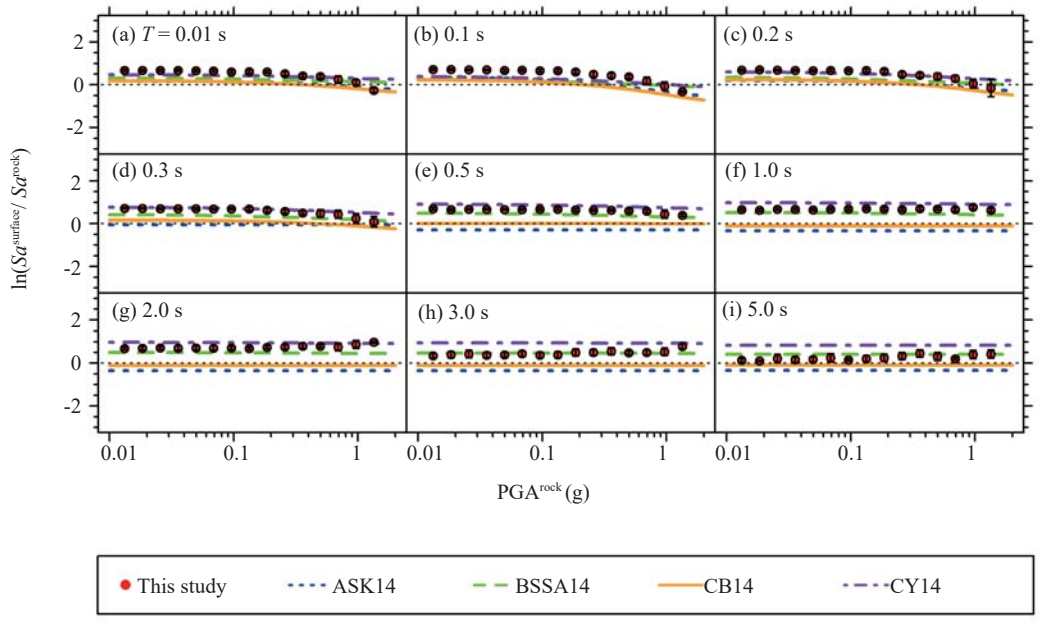

Fig. 11 Amplifications for profiles with a depth of 500 m and a V_{S30} of 455 m/s compared with the amplifications by NGA-West2 GMPEs

surface, the T_S is close to zero, while it is as high as 6 s where deep soft deposits exist in the center of the delta basin.

Figure 15 through Fig. 17 show ground motion amplification maps for various T and PGA^{rock} combinations developed based on the estimated T_S distributions (as shown in Fig. 14). When the PGA^{rock} is small, the amplification shows little variation (close to 2) with respect to the change in T_S at short T (Fig. 15 (a) and (b)), while it shows dramatic change (from 1 to 4) with T_S at long T (Fig. 15 (c) and (d)). This observation is also found from Fig. 13. When the PGA^{rock} is 0.2 g and 0.5 g (Fig. 16 and Fig. 17, respectively), there are de-amplifications of short-period ground motions in the

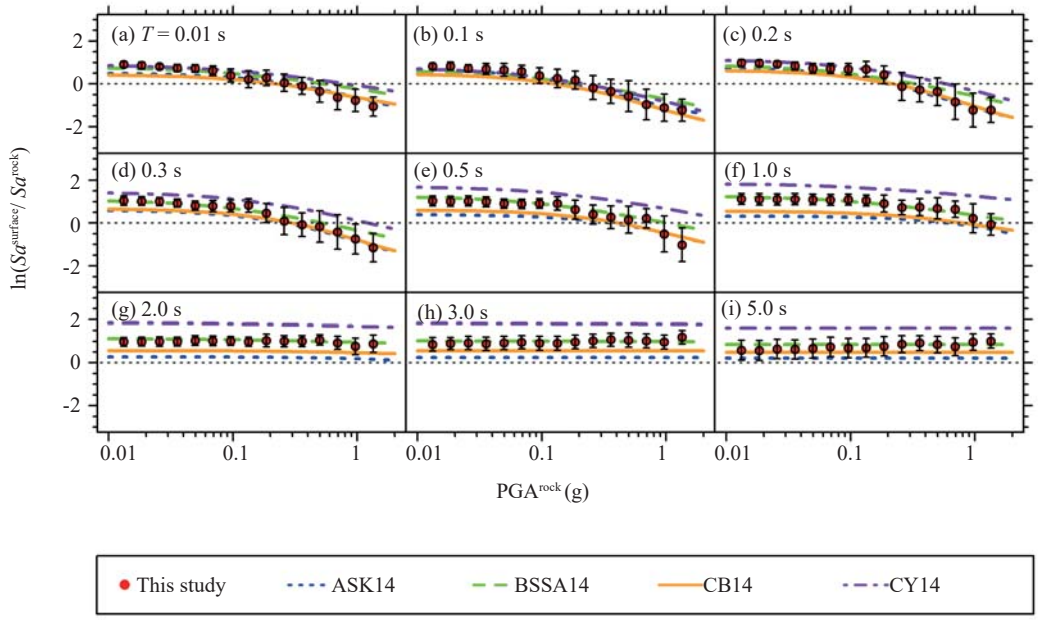

Fig. 12 Amplifications for profiles with a depth of 500 m and a V_{S30} of 208 m/s compared with the amplifications by NGA-West2 GMPEs

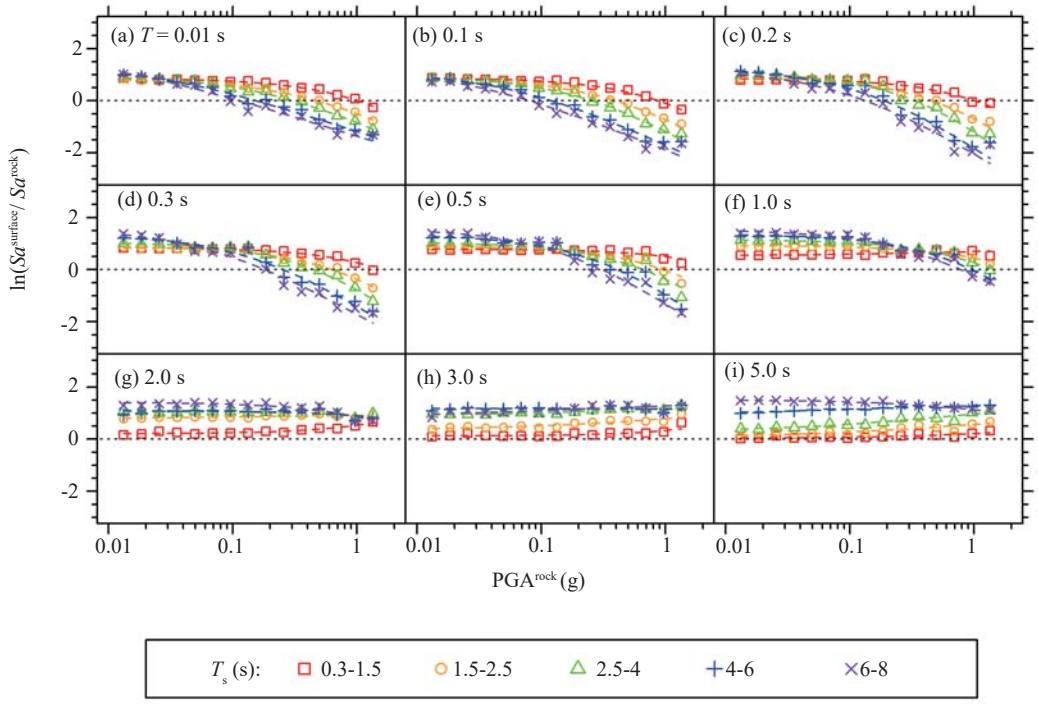

Fig. 13 Mean values of the natural logarithm of ground motion amplifications, ln($Sa^{surface}/Sa^{rock}$), with respect to PGA^{rock} for different site period (T_s) ranges. The smoothed amplifications are shown in dashed lines

center of the basin where T_S is large. The ground motions are substantially amplified at long periods (T = 1 s – 3 s) in the center of the basin for all the PGA^{rock} levels. The amplifications at T = 1 s for a PGA^{rock} of 0.5 g (Fig. 17(c)) do not exhibit the significant variation with T_S because the amplifications for different T_S are similar as shown in Fig. 13(f). From all of the cases, the importance of T_S on the ground motion amplifications is demonstrated. Particularly, the amplification is highest at long periods where the site is soft and deep (long T_S).

5 Conclusions

This study investigated the effects of deep soil deposits on ground motion amplifications for the Fraser River delta in Greater Vancouver, Canada. The shear-wave velocity profiles measured in this region were collected to develop generic profiles for use in 1D site response simulations. Unlike the previous studies, the profiles included a full range of soils from Holocene deposits to Pleistocene glacial deposits. The strong

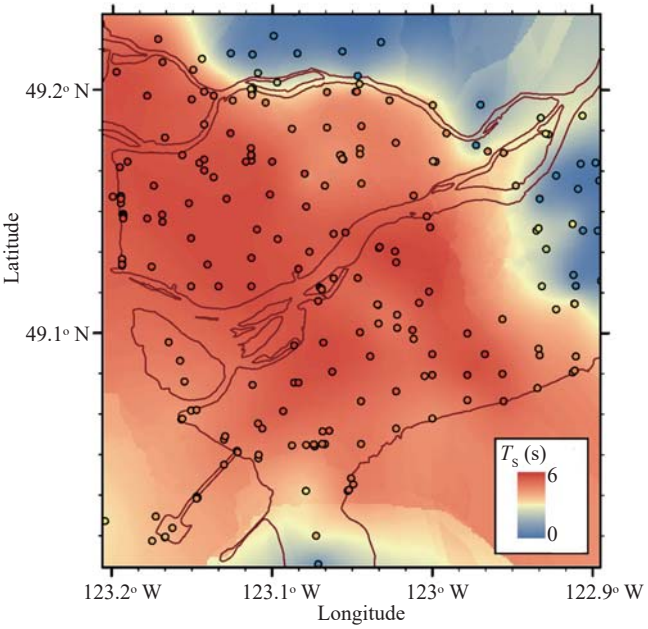

Fig. 14 Site period (T_S) map for the Fraser River delta. Rivers and coastlines are shown in greylines. The circles represent the T_S at the locations of V_S measurements

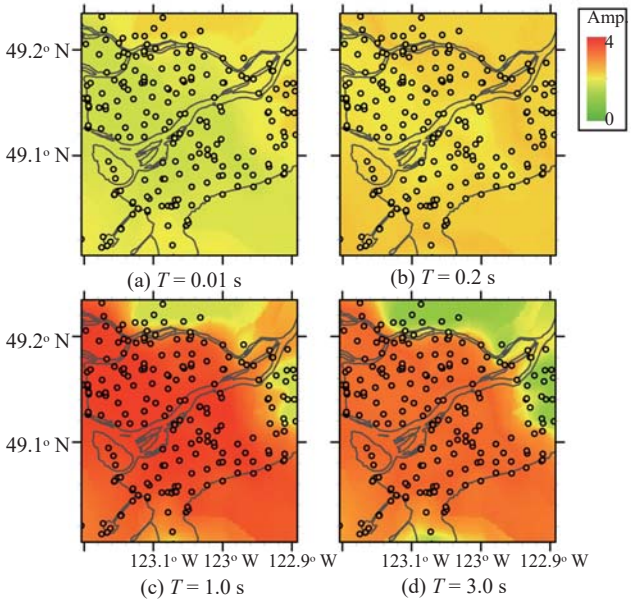

Fig. 15 Ground motion amplification maps for PGA^{rock} = 0.05 g for (a) T=0.01 s; (b) T=0.2 s; (c) T=1.0 s; and (d) T=3.0 s. Rivers and coastlines are shown in grey lines. The circles represent the amplification factors at the locations of V_S measurements

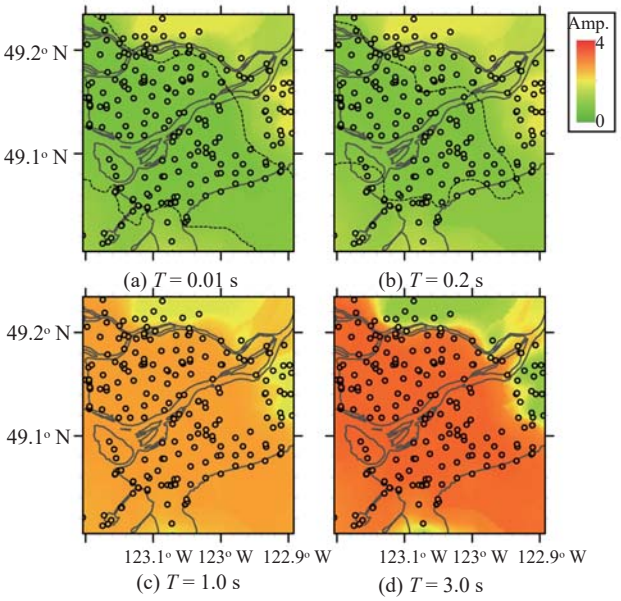

Fig. 16 Ground motion amplification maps for PGA^{rock} = 0.2 g for (a) T=0.01 s; (b) T=0.2 s; (c) T=1.0 s; and (d) T=3.0 s. Rivers and coastlines are shown in grey lines. The circles represent the amplification factors at the locations of V_S measurements. The dashed black lines represent location where the amplification is unity

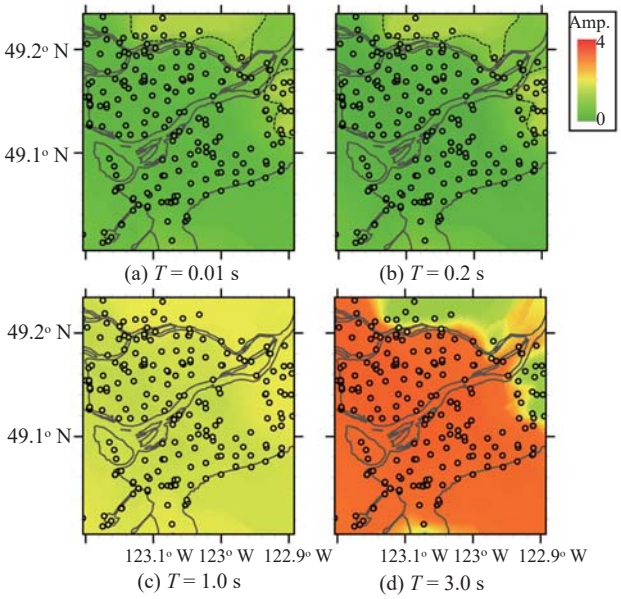

Fig.17 Ground motion amplification maps for PGA^{rock} = 0.5 g for (a) T=0.01 s; (b) T=0.2 s; (c) T=1.0 s; and (d) T=3.0 s. Rivers and coastlines are shown in grey lines. The circles represent the amplification factors at the locations of V_S measurements. The dashed black lines represent location where the amplification is unity

ground motions recorded in California were used as input ground motions. Based on both EL and NL site response simulations, the effects of soil depth (represented by soil period) on ground motion amplification for various spectral periods were clearly demonstrated. At short periods ($T \leq 0.2$ s), ground motion amplifications decrease with PGA^{rock}, and also decrease with T_S, particularly when the PGA^{rock} is larger than 0.1 g. At long periods ($T \geq 2$ s), amplifications barely change with PGA^{rock}, and increase with T_S. For intermediate periods ($T = 0.3$ s – 1 s), the mixed amplification characteristics are observed. The amplifications computed in this study are most comparable with the BSSA14 model among the four NGA-West2 models, and show slightly more nonlinearity at short periods ($T < 1$ s) when a site is soft (e.g., $V_{S30} = 208$ m/s).

In addition to showing the ground motion amplifications in a function of PGA^{rock}, T_S, and spectral period, the ground motion amplification maps for four spectral periods and three PGA^{rock} levels were generated to be used in the regional seismic risk assessment in conjunction with structural vulnerability and exposure values (e.g., values of structures, contents, and business interruption). These maps are useful particularly for system-level analyses of infrastructure such as airports and transportation systems as they cover wide areas.

This study is intended to provide guidance in ground motion amplifications by considering a full range of soil profiles and rock ground motions and using most advanced dynamic soil constitutive model, which has not been available up until now. However, this study only considered the effects of soil depth within the basin (1D effects), and the effects of inclined soil layers at the edge of the basin (3D effects) need to be further investigated in the future. The ground motion amplifications proposed in this study are applicable only to shallow crustal earthquake scenarios. Further investigation is necessary for amplifications of deep crustal, inslab, and subduction zone ground motions.

Acknowledgement

This research was supported by the 2018 Research Fund (1.170059.01) of UNIST (Ulsan National Institute of Science and Technology) and the National Research Foundation of Korea (NRF) with a grant from the Korean government (MSIT) (NRF-2017R1C1B5074430). The author thanks Dr. Hunter for providing the shear-wave velocity profile data, Dr. Emel Seyhan and Dr. Hamed Ashouri for their assistance in processing the shear-wave velocity profile data, and the anonymous reviewers for their detailed and insightful comments that improved the quality of the manuscript.

References

Abrahamson NA, Silva WJ and Kamai R (2014), "Summary of the ASK14 Ground Motion Relation for Active Crustal Regions," *Earthquake Spectra*, **30**(3): 1025–1055.

Ancheta TD, Darragh RB, Stewart JP, Seyhan E, Silva WJ, Chiou BS-J, Wooddell KE, Graves RW, Kottke AR, Boore DM, Kishida T and Donahue JL (2014), "NGA-West2 Database," *Earthquake Spectra*, **30**(3): 989–1005.

Anderson DL, Byrne PM, DeVall RH, Naesgaard E and Wijewickreme D (2007), Geotechnical Design Guidelines for Buildings on Liquefiable Sites in Accordance with NBC 2005 for Greater Vancouver region, *Greater Vancouver Liquefaction Task Force Report*, University of British Columbia: 74 pages.

Atkinson GM and Cassidy JF (2000), "Integrated Use of Seismograph and Strong-Motion Data to Determine Soil Amplification: Response of the Fraser River Delta to the Duvall and Georgia Strait Earthquakes," *Bulletin of the Seismological Society of America*, **90**(4): 1028–1040.

Boore DM, Stewart JP, Seyhan E and Atkinson GM (2014), "NGA-West2 Equations for Predicting PGA, PGV, and 5% Damped PSA for Shallow Crustal Earthquakes," *Earthquake Spectra*, **30**(3): 1057–1085.

Britton J, Harris J, Hunter J and Luternauer J (1995), "The Bedrock Surface Beneath the Fraser River Delta in British Columbia Based on Seismic Measurements," Current Resarch 1995-E, Geological Survey of Canada: 83–89.

Campbell KW and Bozorgnia Y (2013), *NGA-West2 Campbell-Bozorgnia Ground Motion Model for the Horizontal Components of PGA, PGV, and 5%-Damped Elastic Pseudo-Acceleration Response Spectra for Periods Ranging from 0.01 to 10 s*, Pacific Earthquake Engineering Research Center, University of California, Berkeley: 75 pages.

Campbell KW and Bozorgnia Y (2014), "NGA-West2 Ground Motion Model for the Average Horizontal Components of PGA, PGV, and 5% Damped Linear Acceleration Response Spectra," *Earthquake Spectra*, **30**(3): 1087–1115.

Cassidy JF and Rogers GC (1999), "Seismic Site Response in the Greater Vancouver, British Columbia, Area: Spectral Ratios from Moderate Earthquakes," *Canadian Geotechnical Journal*, **36**(2): 195–209.

Cassidy JF and Rogers GC (2004), "Variation in Ground Shaking on the Fraser River Delta (Greater Vancouver, Canada) from Analysis of Moderate Earthquakes," *Proceedings of the 13th World Conference on Earthquake Engineering*, Vancouver, B.C., Canada: 7 pages.

Cassidy JF, Rogers GC and Weichert DH (1997), "Soil Response on the Fraser Delta to the $M_W = 5.1$ Duvall, Washington, Earthquake." *Bulletin of the Seismological Society of America*, **87**(5): 1354–1361.

Chenari RJ and Bostani Taleshani SA (2016), "Site Response of Heterogeneous Natural Deposits to Harmonic Excitation Applied to More Than 100 Case

Histories," *Earthquake Engineering and Engineering Vibration*, **15**(2): 341–356.

Chiou BS-J and Youngs RR (2014), "Update of the Chiou and Youngs NGA Model for the Average Horizontal Component of Peak Ground Motion and Response Spectra," *Earthquake spectra*, **30**(3): 1117–1153.

Clague JJ, Luternauer JL and Mosher DC (1998), *Geology and Natural Hazards of the Fraser River Delta*, British Columbia, Geological Survey of Canada (Bulletin 525): 270 pages.

Dallimore SR, Edwardson KA, Hunter JA, Lutenauer JL and Clague JJ (1996), *Lithologic, Geotechnical and Geophysical Logs from a Deep Borehole at Richmond City Hall*, British Columbia. GSC Open File 3356.

Darendeli MB (2001), Development of a New Family of Normalized Modulus Reduction and Material Damping Curves. *Civil Engineering*, Austin, University of Texas at Austin: 395.

Ewald M, Igel H, Hinzen K-G and Scherbaum F (2006), "Basin-Related Effects on Ground Motion for Earthquake Scenarios in the Lower Rhine Embayment," *Geophysical Journal International*, **166**(1): 197–212.

Finn WDL, Zhai E, Thavaraj T, Hao XS and Ventura CE (2003), "1-D and 2-D Analyses of Weak Motion Data in Fraser Delta from 1996 Duvall Earthquake," *Soil Dynamics and Earthquake Engineering*, **23**(4): 323–329.

Frankel A, Stephenson W and Carver D (2009), "Sedimentary Basin Effects in Seattle, Washington: Ground-Motion Observations and 3D Simulations," *Bulletin of the Seismological Society of America*, **99**(3): 1579–1611.

Graizer V (2016), "Ground-Motion Prediction Equations for Central and Eastern North America," *Bulletin of the Seismological Society of America*, **106**(4): 1600–1612.

Groholski DR, Hashash YMA, Kim B, Musgrove M, Harmon J and Stewart JP (2016), "Simplified Model for Small-Strain Nonlinearity and Strength in 1D Seismic Site Response Analysis," *Journal of Geotechnical and Geoenvironmental Engineering*, **142**(9): 04016042.

Hashash YMA, Musgrove MI, Harmon JA, Groholski DR, Phillips CA and Park D (2015), DEEPSOIL 6.1, User Manual: 104.

Hunter J, Dallimore S and Christian H (1997), "Borehole Measurements of Shear Wave Velocity Discontinuities in Quaternary Sediments, Fraser River Delta, British Columbia," *Current Research 1997-A*, Geological Survey of Canada: 159–165.

Hunter JA, Burns RA, Good RL and Pelletier CF (1998), "A Compilation of Shear Wave Velocities and Borehole Geophysics Logs in Unconsolidated Sediments of the Fraser River Delta," British Columbia, Geological Survey of Canada, *Open File 3622*: 13 pages.

Hunter JA and Christian HA (2001), "Use of Shear Wave Velocities to Estimate Thick Soil Amplification Effects in the Fraser River Delta, British Columbia," *Proceedings of the Symposium on the Application of Geophysics to Environmental and Engineering Problems* (*SAGEEP*), March 4-7, 2011, Denver, Colorad.

Kaklamanos J, Bradley BA, Thompson EM and Baise LG (2013), "Critical Parameters Affecting Bias and Variability in Site-Response Analyses Using KiK-net Downhole Array Data," *Bulletin of the Seismological Society of America*, **103**(3): 1733–1749.

Kim B and Hashash YMA (2013), "Site Response Analysis Using Downhole Array Recordings during the March 2011 Tohoku-Oki Earthquake and the Effect of Long-Duration Ground Motions," *Earthquake Spectra*, **29**(S1): S37–S54.

Kim B, Hashash YMA, Stewart JP, Rathje EM, Harmon JA, Musgrove MI, Campbell KW and Silva WJ (2016), "Relative Differences between Nonlinear and Equivalent-Linear 1-D Site Response Analyses," *Earthquake Spectra*, **32**(3): 1845–1865.

Kim B and Shin M (2017), "A Model for Estimating Horizontal Aftershock Ground Motions for Active Crustal Regions," *Soil Dynamics and Earthquake Engineering*, **92**: 165–175.

Ladd CC (1991), "Stability Evaluation during Staged Construction," *Journal of Geotechnical Engineering*, **117**(4): 540-615.

Li C, Li H, Hao H, Bi K and Tian L (2018), "Simulation of Multi-Support Depth-Varying Earthquake Ground Motions within Heterogeneous Onshore and Offshore Sites," *Earthquake Engineering and Engineering Vibration*, **17**(3): 475–490.

Liang F, Chen H and Huang M (2017), "Accuracy of Three-Dimensional Seismic Ground Response Analysis in Time Domain Using Nonlinear Numerical Simulations," *Earthquake Engineering and Engineering Vibration*, **16**(3): 487–498.

Liu H, Bo J, Li P, Qi W and Zhang Y (2016), "Site Amplification Effects as an Explanation for the Intensity Anomaly in the Hanyuan Town during the Wenchuan M_w7.9 Earthquake," *Earthquake Engineering and Engineering Vibration*, **15**(3): 435–444.

Mazzotti S, Lambert A, Van der Kooij M and Mainville A (2009), "Impact of Anthropogenic Subsidence on Relative Sea-Level Rise in the Fraser River Delta," *Geology*, **37**(9): 771–774.

Molnar S, Cassidy JF, Olsen KB, Dosso SE and He J (2014a), "Earthquake Ground Motion and 3D Georgia Basin Amplification in Southwest British Columbia: Deep Juan de Fuca Plate Scenario Earthquakes," *Bulletin of the Seismological Society of America*, **104**(1): 301–320.

Molnar S, Cassidy JF, Olsen KB, Dosso SE and He J (2014b), "Earthquake Ground Motion and 3D Georgia Basin Amplification in Southwest British Columbia:

Shallow Blind-Thrust Scenario Earthquakes," *Bulletin of the Seismological Society of America*, **104**(1): 321–335.

Phillips C and Hashash YMA (2009), "Damping Formulation for Non-Linear 1D Site Response Analyses," *Soil Dynamics and Earthquake Engineering*, **29**(7): Pages 1143–1158.

Sihua Z and Lung WY (2004), "Seismic Ground Motion Relationship in Southern China Based on Stochastic Finite-Fault Model," *Earthquake Engineering and Engineering Vibration*, **3**(1): 11–21.

Uthayakumar UM and Naesgaard E (2004), "Ground Response Analysis for Seismic Design in Fraser River Delta, British Columbia," *13th World Conference on Earthquake Engineering*, Vancouver, B.C., Canada, Augus 1-6, 2004, Paper No. 2104.

Vaez Shoushtari A, Adnan AB and Zare M (2018), "Ground Motion Prediction Equations for Distant Subduction Interface Earthquakes Based on Empirical Data in the Malay Peninsula and Japan," *Soil Dynamics and Earthquake Engineering*, **109**: 339–353.

Walling M, Silva W and Abrahamson N (2008), "Nonlinear Site Amplification Factors for Constraining the NGA Models," *Earthquake spectra*, **24**(1): 243–255.

Wang H, Xie L, Wang S and Ye P (2013), "Site Response in the Qionghai Basin in the Wenchuan earthquake," *Earthquake Engineering and Engineering Vibration*, **12**(2): 195–199.

Wijewickreme D (2010), "Cyclic Sheaer Response of Low Plastic Fraser River silt," *Proceedings of the 9th U.S. National and 10th Canadian Conference on Earthquake Engineering*, July 25-29, 2010, Toronto, Ontario, Canada , Paper No 1431.

Wong YL, Zhao JX and Luo Q (2002), "Attenuation Characteristics of Ground Motions in Northern China," *Earthquake Engineering and Engineering Vibration*, **1**(2): 161–166.

Appendix

Figures A.1 through A.6 show data, means, and standard deviations of ground motion amplifications from the simulations at multiple periods and site periods (T_S). Figure A. 7 shows ground motion amplifications, $\ln(Sa^{surface}/Sa^{rock})$, with respect to PGA^{rock} for different site period (T_S) ranges using two different methods::equivalent-linear (EL) and nonlinear (NL) site response analyses. This figure clearly demonstrates the effects of the nonlinear behavior of the soils on ground motion amplifications. The nonlinear site response analyses resulted in stronger de-amplifications when PGA^{rock} is larger than 0.2 g.

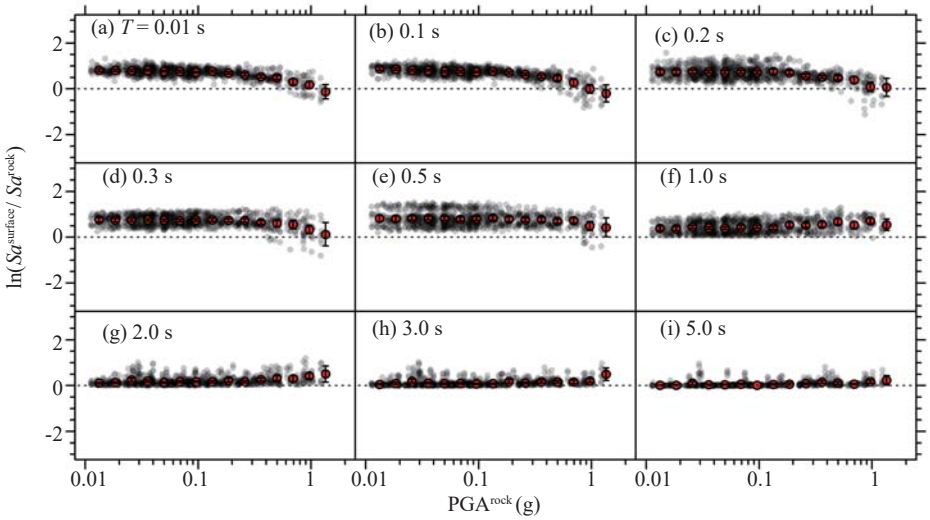

Fig. A1 Amplifications for site period (T_S) of 0.3 to 0.8 s. Grouped mean and mean ± one standard deviation are shown in red circles and error bars

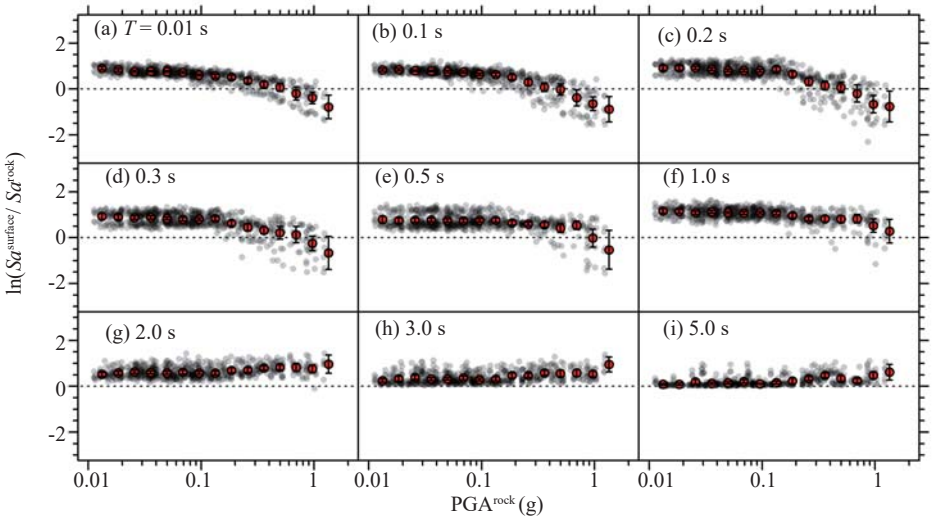

Fig. A2 Amplifications for site period (T_S) of 0.8 to 1.5 s. Grouped mean and mean ± one standard deviation are shown in red circles and error bars

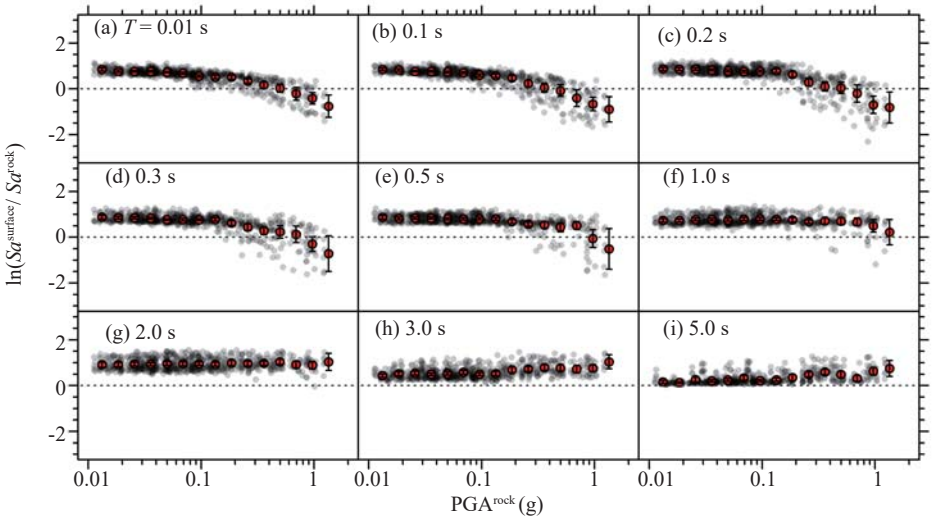

Fig. A3 Amplifications for site period (T_S) of 1.5 to 2.5 s. Grouped mean and mean ± one standard deviation are shown in red circles and error bars

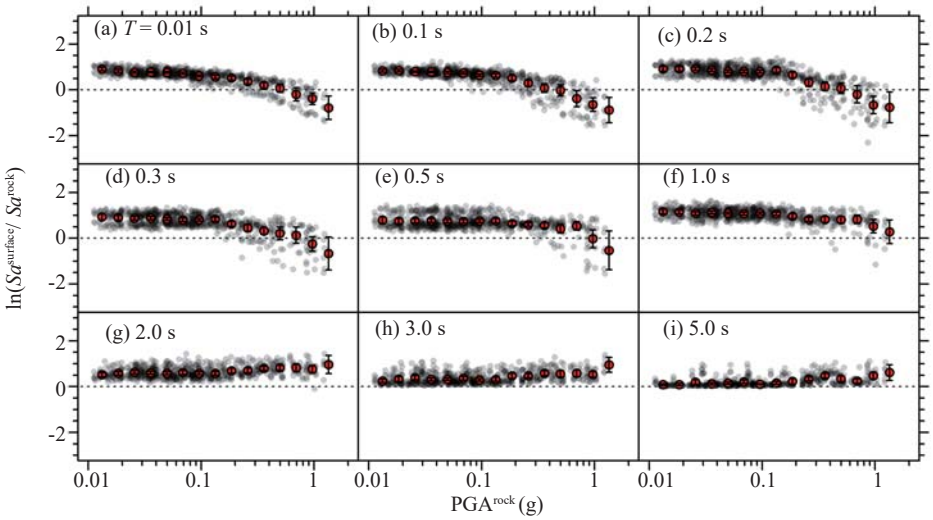

Fig. A4 Amplifications for site period (T_S) of 2.5 to 4 s. Grouped mean and mean ± one standard deviation are shown in red circles and error bars

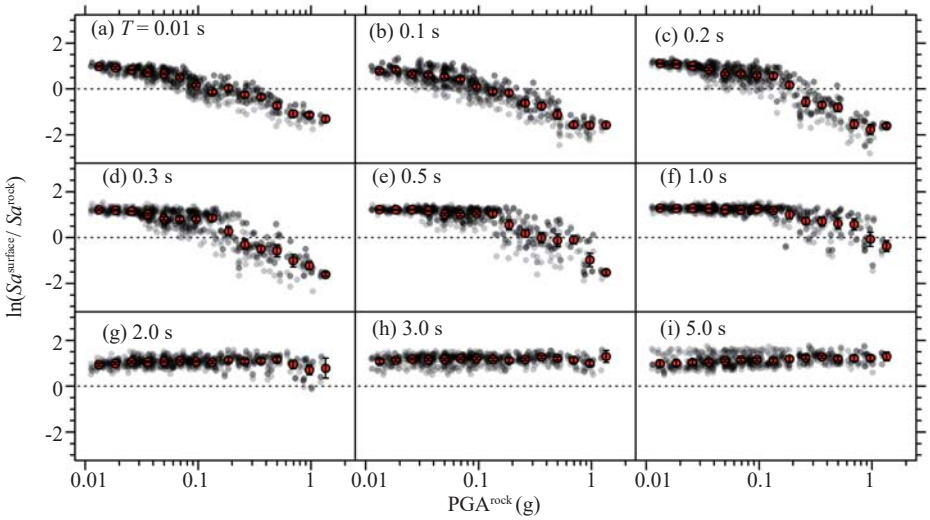

Fig. A5 Amplifications for site period (T_S) of 4 to 6 s. Grouped mean and mean ± one standard deviation are shown in red circles and error bars

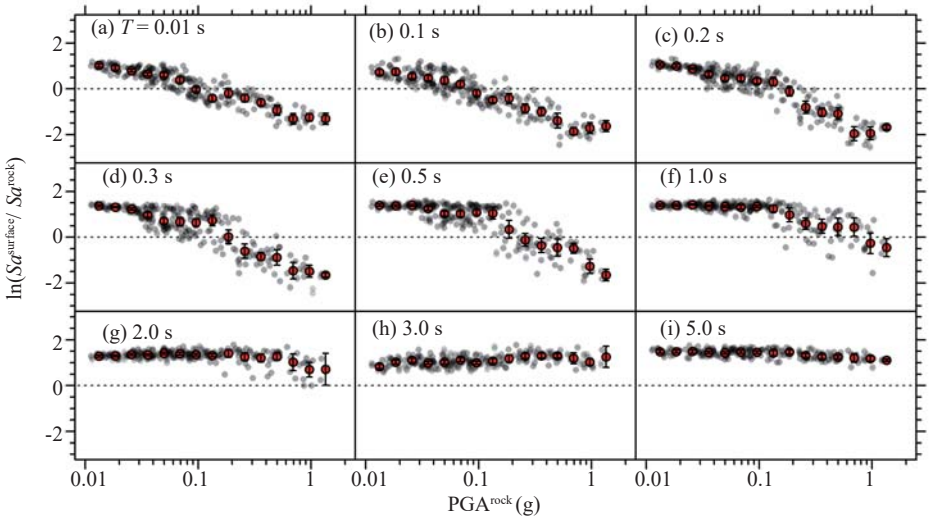

Fig. A6 Amplifications for site period (T_S) of 6 to 8 s. Grouped mean and mean ± one standard deviation are shown in red circles and error bars

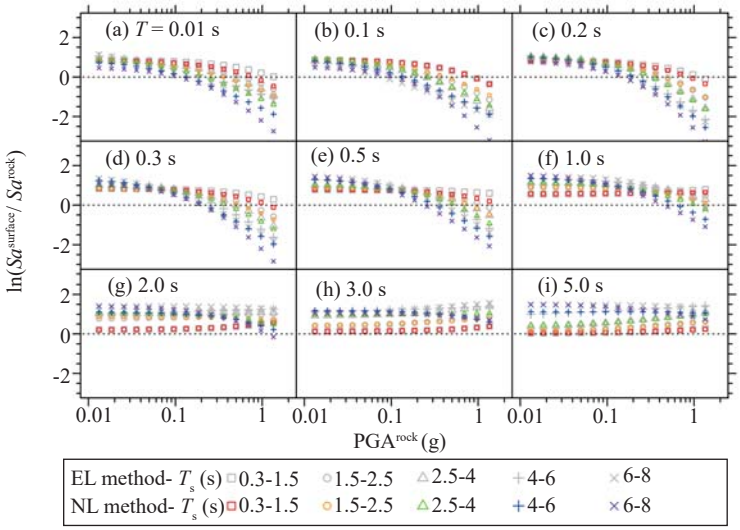

Fig. A7 Mean values of ground motion amplifications, $\ln(S_a^{surface}/S_a^{rock})$, with respect to PGA^{rock} for different site period (T_s) ranges using two different methods: equivalent-linear (EL) and nonlinear (NL) site response analyses